ACS APPLIED MATERIALS & INTERFACES

Research Article

www.acsami.org

Two-Dimensional Titanium Carbide for Efficiently Reductive Removal of Highly Toxic Chromium(VI) from Water

Yulong Ying,[†] Yu Liu,[†] Xinyu Wang,[†] Yiyin Mao,[†] Wei Cao,[†] Pan Hu,[†] and Xinsheng Peng*[,†,‡]

[†]State Key Laboratory of Silicon Materials, Department of Materials Science and Engineering, and [‡]Cyrus Tang Center for Sensor Materials and Application, Department of Materials Science and EngineeringZhejiang University, Hangzhou 310027 P. R. China

Supporting Information

ABSTRACT: Two dimensional (2-D) $Ti_3C_2T_x$ nanosheets are obtained by etching bulk $Ti_3C_2T_x$ powders in HF solution and delaminating ultrasonically, which exhibit excellent removal capacity for toxic Cr(VI) from water, due to their high surface area, well dispersibility, and reductivity. The $Ti_3C_2T_x$ nanosheets delaminated by 10% HF solution present more efficient Cr(VI) removal performance with capacity of 250 mg g^{-1}, and the residual concentration of Cr(VI) in treated water is less than 5 ppb, far below the concentration (0.05 ppm) of Cr(VI) in the drinking water standard recommended by the World Health Organization. This kind of 2-D $Ti_3C_2T_x$ nanosheet can not only remove Cr(VI) rapidly and effectively in one step from aqueous solution by reducing Cr(VI) to Cr(III) but also adsorb the reduced Cr(III) simultaneously. Furthermore, these reductive 2-D $Ti_3C_2T_x$ nanosheets are generally explored to remove other oxidant agents, such as $K_3[Fe(CN)_6]$, $KMnO_4$, and $NaAuCl_4$ solutions, by converting them to low oxidation states. These significantly expand the potential applications of 2-D $Ti_3C_2T_x$ nanosheets in water treatment.

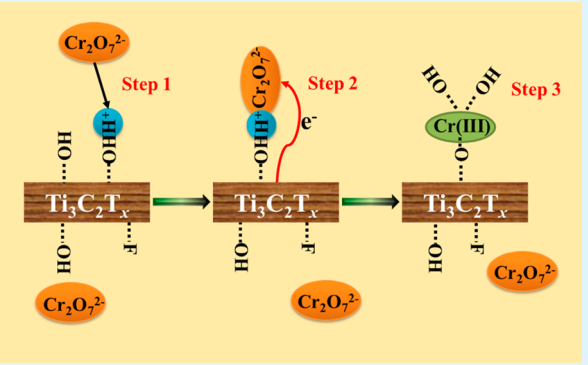

KEYWORDS: *two-dimensional, titanium carbide, Cr(VI), reductive removal*

1. INTRODUCTION

Two-dimensional (2-D) materials, such as graphene and its derivative, metal chalcogenides, transition metal oxides, and other 2-D compounds have historically been one of the most extensively studied classes of materials.[1] Due to their fascinating properties, these 2-D materials can potentially lead to a variety of promising applications such as optoelectronics, catalysts, spintronics, solar cells, biological and chemical sensors, supercapacitors, and lithium ion batteries.[2] Moreover, these 2-D materials also demonstrate great potential for water treatment where they are used as separation membranes.[3−6]

Recently, a new family of 2-D materials, named MXenes, has attracted raising attention, because of their good structural stabilities, excellent electrical conductivities and environmentally friendly characteristics.[7−10] Ti_3AlC_2 is the most studied MAX[11] ("M" is an early transition metal, "A" is an A group, mostly group 13 and 14 element, and "X" is C and/or N.) material in this big family. To date the exfoliated 2-D $Ti_3C_2T_x$ (T= OH or F) nanosheets have been widely studied in energy storage applications such as lithium-ion batteries,[8,10,12] supercapacitors,[9] and fuel cells.[13,14] Recently, Peng and coworkers found that titanium carbide with Ti surfaces covered with hydroxyl and fluorine treated with alkalization intercalation exhibit unique adsorption behavior for toxic Pb(II).[15]

Hexavalent chromium, one of the heavy metal elements, is a powerful oxidant and widely used in industrial processes, such as electroplating, water cooling, leather tanning, and metal finishing.[16] The effluents from these industries contain abundant residual Cr(VI) which, if discharged without proper nonhazardous treatment, will cause great contamination to groundwater and are highly toxic to plants, animals, and the human body.[17] The World Health Organization (WHO) recommends that the levels of Cr(VI) in drinking water should be reduced to 0.05 ppm,[18] which is 5-fold higher than that in the State of California (0.01 ppm).[19] Compared with Cr(VI), Cr(III) is 1000-fold less toxic and readily precipitated as $Cr(OH)_3$ because of its low solubility.[20]

The typical procedure to eliminate the toxicity of Cr(VI) in industry is reduction of Cr(VI) to Cr(III) by various chemical reagents, such as sulfur dioxide gas, sodium bisulfite, and iron salts,[21] followed by its precipitation as Cr(III) hydroxide in the near-neutral solution. However, this strategy often generates large amounts of secondary waste products and costs large amounts of acids or bases to adjust the pH of the solution.[22] Numerous other methods have been reported to remove Cr(VI) from water, such as ion exchange,[23] reverse osmosis,[24] electrodialysis,[25] and adsorption.[26] Nevertheless, many of these approaches are marginally cost-effective or difficult to meet minimum standard as a drinking water (WHO, 0.05 ppm) or even as agricultural use (Chinese standard, 0.1 ppm). Thus,

Received: October 27, 2014
Accepted: January 5, 2015
Published: January 5, 2015

DOI: 10.1021/am5074722
ACS Appl. Mater. Interfaces 2015, 7, 1795−1803

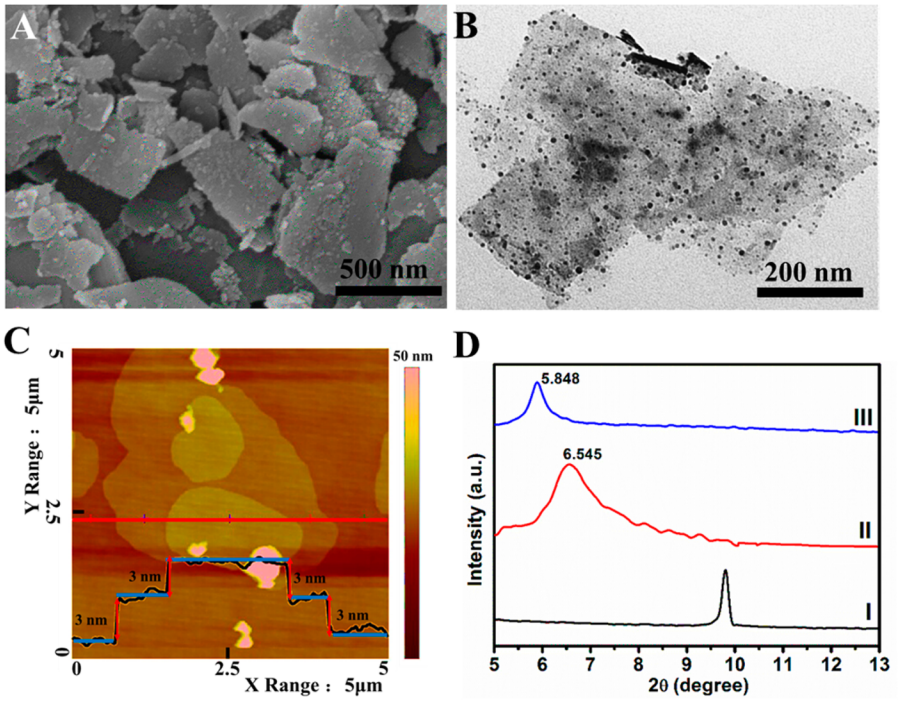

Figure 1. (A) SEM image, (B) TEM image, and (C) AFM image of $Ti_3C_2T_x$-10% nanosheets after fully exfoliated. (D) The XRD patterns of the $Ti_3C_2T_x$-10% sample at different states: (I) as received without HF treatment, (II) after 10% HF treatment, and (III) after fully exfoliated.

upon the viewpoint of practical application, it was desirable to find a new environment-friendly material that can fast and effectively remove Cr(VI) in a facile way as well as the product, Cr(III).

For the first time, after etching away the Al layer and exfoliation to 2-D nanosheets, we found that these 2-D $Ti_3C_2T_x$ nanosheets demonstrate a new promising function for environmental pollutant decontamination because of their reducibility, well dispersibility and large specific surface area (SSA). These 2-D $Ti_3C_2T_x$ nanosheets with Ti-surfaces covered with hydroxyl and fluorine exhibited unique reductive removal performance for toxic Cr(VI). The residual concentration of Cr(VI) in treated water could be low, down to less than 5 ppb, meeting the standard for purified drinking water (WHO standard, 0.05 ppm).[18] In addition, the produced Cr(III) ions were simultaneously removed from water at pH 5.0 by in situ adsorption[22] with the assistance of Ti−O bond. These 2-D $Ti_3C_2T_x$ nanosheets present a general way for reductive removal of toxic oxidant agents from water and provide a unique way to precipitate noble metal, such as Au, on the surface of $Ti_3C_2T_x$ nanosheets by simple in situ reduction.

2. EXPERIMENTAL SECTION

2.1. Preparation of $Ti_3C_2T_x$ Nanosheets. Ti_3AlC_2 powders (>98 wt % purity; particle size <75 μm, i.e., 200 mesh) were purchased from Beijing Jinhezhi Materials Co,. Ltd. The Ti_3AlC_2 powder was immersed in HF (Sinopharm Chemical Reagent Co., Ltd. 50 wt %) solutions of different concentrations at 300 K by stirring for 24 h. Then the resulting suspension was washed by deionized water for several times and centrifuged to remove the remaining impurities and HF until the solution reached a pH of 5−6. The wet sediment was washed twice using ethanol and moved to a wide-mouth jar to dry in air for 3−4 days, named as $Ti_3C_2T_x$. The multilayered $Ti_3C_2T_x$ was then stirred with dimethyl sulfoxide (DMSO) (Sinopharm Chemical Reagent Co., Ltd.) at 310 K for 24 h. The colloidal suspension was centrifuged to obtain the intercalated powders. And then, the powders were washed with deionic water several times to remove the residue DMSO. Next, the residue was dispersed in deionic water in a weight ratio of $Ti_3C_2T_x$ to water of 1:100. Afterward, ultrasonication was carried out to exfoliate the $Ti_3C_2T_x$ into 2-D sheets for 4 h under argon. The suspension was centrifuged for 10 min with 3500 rpm to remove the unexfoliated MXene. Finally, the $Ti_3C_2T_x$ nanosheets were obtained by filtration and dried in vacuum for further experiments. After fully exfoliation, the prepared $Ti_3C_2T_x$ nanosheets prepared by HF solution with weight percent of 50%, 25%, and 10%, were named as $Ti_3C_2T_x$-50%, $Ti_3C_2T_x$-25%, and $Ti_3C_2T_x$-10%, respectively.

The $Ti_3C_2T_x$-10% balck suspension was converted to white precipites after stored in beaker for 3 months under atmosphere condition.

2.2. Characterization. The X-ray diffraction (XRD) patterns were obtained with a powder X-ray diffract meter (SHIMAZU XRD-6000) with Cu Ka radiation (λ = 1.5406 Å) at a generator voltage of 40 kV and a generator current of 40 mA with a scanning speed of 4° min^{-1} at room temperature. Silicon single crystal oriented along the ⟨100⟩ direction is used to calibrate the XRD diffraction angles. The morphology of the samples was recorded by scanning electron microscope (SEM) (Hitachi S-4800) at 5 kV and transmission electron microscope (TEM) (Philips CM200) with an accelerating voltage of 160 kV. Tapping mode atomic force microscope (AFM) images were obtained by MultiMode scanning probe microscope (SPM, VEECO). For AFM observation, the samples were prepared by depositing one droplet of the corresponding suspension on single crystal silicon substrate and dried at room temperature. X-ray photoelectron spectroscopy (XPS) analyses of the prepared samples were recorded with a X-ray photoelectron spectrometer (Thermo Scientific ESCALAB-250Xi) with a Al Ka X-ray source. The SSA of the samples were evaluated by nitrogen sorbtion and desorption using a Quantachrome Autosorb-1 apparatus by Brunauer−Emmett−Teller (BET) method. Zeta potentials were measured by dynamic light scattering (DLS, Zetasizer3000HSA, Malvern Instruments, UK) method at desired solution pH, 2.0−13.0.

2.3. Removal of Cr(VI). The stock solution of 100 mM Cr(VI) was prepared by dissolving $K_2Cr_2O_7$ in deionic water. Then this stock solution was diluted to the desired concentration and pH. The pH was adjusted using hydrochloric acid and sodium hydroxide solution. All

DOI: 10.1021/am5074722
ACS Appl. Mater. Interfaces 2015, 7, 1795−1803

the removal experiments were carried out at room temperature for 3 days.

In order to exclude the uncertain influences on solution pH after adding the $Ti_3C_2T_x$ sample into $K_2Cr_2O_7$ solution, $Ti_3C_2T_x$ nanosheets suspension with equal volume and same pH as that of $K_2Cr_2O_7$ solution was used. In the removal capacity test, 200 mL $Ti_3C_2T_x$-10% suspensions (pH 5.0, concentration 0.6 g L^{-1}), were added to 800 mL beakers containing 200 mL Cr(VI) solution (4 mM, 208 ppm, pH 5.0). The mixing solution is stirred for 3 days to ensure a complete reaction. Then, the mixture was filtered through 0.2 μm polycarbonate membrane. Similar processes were carried out for $Ti_3C_2T_x$-25% and $Ti_3C_2T_x$-50%, respectively. The concentration of the residue Cr(VI) was characterized by a UV−vis spectrophotometer at 540 nm using 5-diphenyl carbazide method. The total concentration of Cr was characterized by a coupled plasma-atomic emission spectrometer (ICP-AES). The effect of amount of $Ti_3C_2T_x$-10% nanosheets on Cr(VI) removal performance was performed in a 800 mL beaker. After mixing 200 mL of Cr(VI) solution (4 mM, 208 ppm, pH 5.0) with 200 mL of $Ti_3C_2T_x$-10% suspension with various concentrations (0.4 g L^{-1}, 0.6 g L^{-1}, 0.8 g L^{-1}, and 2.0 g L^{-1}, pH 5.0), respectively, the concentration of Cr(VI) at various time intervals was recorded by UV−vis spectroscopy. In order to stop the redox reaction, the powders were separated from solution immediately by filtration. The pH effect on Cr(VI) removal performance by $Ti_3C_2T_x$-10% nanosheets was carried out by mixing 200 mL of $Ti_3C_2T_x$-10% nanosheets suspension (0.8 g L^{-1}) with 200 mL of Cr(VI) solution (208 ppm) at different pHs (pH 2.0, 5.0, 7.0, 10.0, 13.0), respectively.

2.4. Reductive Removal of Other Oxidants. The $Ti_3C_2T_x$-10% suspension was mixed with $K_3[Fe(CN)_6]$ (100 mM), $KMnO_4$ (100 mM), and $NaAuCl_4$ (10 mM) solutions, respectively, to verify the removal ability. The concentration of the residue oxidant was monitored by a UV−vis spectrophotometer, and the concentration of the product of reduction was measured by ICP-AES. The Cr(III) removal ability of $Ti_3C_2T_x$-10% nanosheets was carried out by mixing $Ti_3C_2T_x$-10% nanosheets suspension with $CrCl_3$ (2 mM) at pH 5.0.

3. RESULTS AND DISCUSSION

3.1. Morphology and Structure of $Ti_3C_2T_x$ Nanosheets. Layered $Ti_3C_2T_x$ nanosheets have been prepared by exfoliating bulk Ti_3AlC_2 powders in HF aqueous solution.[7,10] Here, HF solutions with different concentrations were employed for exfoliation of Ti_3AlC_2 powders. After immersed in HF solution for 24 h, the Ti_3AlC_2 powders (200 mesh, Supporting Information (SI), Figure S1) were successfully expanded and converted to layered $Ti_3C_2T_x$ structures (SI, Figure S2A-C). The emergence of layers was caused by etching away the Al layers in Ti_3AlC_2 particles, and the interspace between the layers was enlarged by released H_2.[10] After intercalating by dimethyl sulfoxide (DMSO), the layered structures were further delaminated to 2-D $Ti_3C_2T_x$ nanosheets by sonication (Figure 1A, $Ti_3C_2T_x$-10%, SI, Figure S2D $Ti_3C_2T_x$-50% and 2E $Ti_3C_2T_x$-25%). The sheet-like structures of that treated by 10% HF solutions ($Ti_3C_2T_x$-10%, Figure 1A) are further clearly seen in the cross-section SEM image (SI, Figure S2F) and TEM image (Figure 1B). Figure 1C, the corresponding AFM image, shows that the thickness of $Ti_3C_2T_x$-10% nanosheets is about 3 nm, which is 2 times that of the single layer, since the layer spacing along the *c*-axis is about 1.51 nm, calculated by the XRD pattern in Figure 1D (2θ = 5.848°). The single layer distance agrees with that reported.[15] The average lateral dimension of $Ti_3C_2T_x$-10% nanosheets is around 0.5 μm, statistically measured from hundreds of sheets (SI, Figure S3).

The delaminating and exfoliating processes were further verified by XRD (Figure 1D and Figure 2). The etching away of Al from Ti_3AlC_2 is revealed by the vanishing of the (104) peak at 39° (Figure 2).[8,10] Concomitantly, the shift of the (002) diffraction peak at 9.8° to low angle direction confirms the occurrence of intercalation and delamination processes (Figure 1D), as Al is replaced by OH and F. These are confirmed by the XPS results (Figure 3, SI, Figures S4 and S5, and Table 1), which is consistent with those reported elsewhere.[10,27] Stacked $Ti_3C_2T_x$ multilayers are separated into 2-D $Ti_3C_2T_x$ nanosheets. XRD patterns (Figure 2) show that the Ti_3AlC_2 treated by 10% HF solution and after full exfoliation have the largest layer distance, indicating that a low concentration of HF solution is more suitable for the intercalation and delamination. This might be that high concentration HF solution would dissolve the MAX/MXene powders or form ternary fluorides, which likely affect the intercalation process.[7]

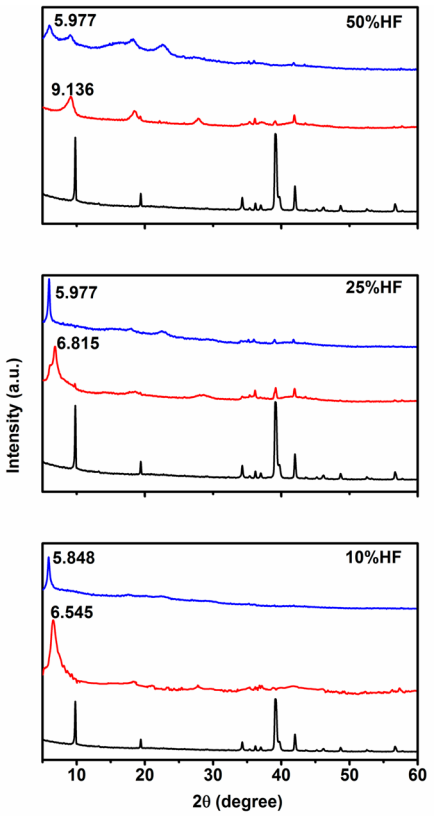

Figure 2. XRD patterns of the Ti_3AlC_2 sample after treated by 50, 25, and 10 wt % HF solution, respectively. Ti_3AlC_2 powders (black line), etching by HF (red lines) and after full exfoliation of $Ti_3C_2T_x$ (blue line).

Chemical compositions of the 2-D nanosheets before and after exfoliation were characterized by XPS. No Al but F in XPS spectra is recorded from $Ti_3C_2T_x$ samples (Table 1 and SI, Figure S5), indicating the full removal of Al and the introduction of F. The single peak of F 1s located at 684.6 eV is assigned to the F ions, SI, Figure S5, which is physically adsorbed on the surface of 2-D $Ti_3C_2T_x$ nanosheets.[28] The amount of F is calculated to be about 10.8 at%. Ti 2p and C 1s spectra before and after 10% HF treatment are shown in Figures 3 and 4. The absence of a Ti−Al bond at around 453 eV and the presence of a C−O bond after HF treatment clearly indicate the Al layers are etching away and $Ti_3C_2T_x$ (T = OH and F) is formed.[7,29]

The exfoliated $Ti_3C_2T_x$ nanosheets can be dispersed very well in water. However, we found that white precipitates appeared slowly in the black exfoliated $Ti_3C_2T_x$ nanosheets aqueous dispersion at atmospheric conditions after 3 months.

DOI: 10.1021/am5074722
ACS Appl. Mater. Interfaces 2015, 7, 1795−1803

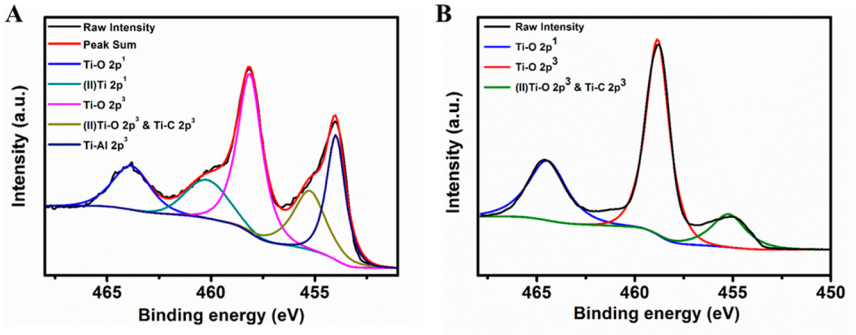

Figure 3. (A) Ti 2p spectrum of the Ti_3AlC_2 sample without any treatment. (B) Ti 2p spectrum of Ti_3AlC_2 sample after treating with 10 wt % HF solution and fully exfoliated.

Table 1. Average Chemical Compositions of the Samples under Different States

	elements (at. %)					
sample	Ti	Al	C	O	F	Cr
Ti_3AlC_2	50.20	15.70	32.40	1.70	*a*	*a*
$Ti_3C_2T_x$	41.26	*a*	28.11	19.89	10.74	*a*
$Ti_3C_2T_x$-Cr	36.34	*a*	24.98	24.79	4.58	9.31
Ti_3C_2-long time	25.02	*a*	16.62	50.31	8.05	*a*

[a]No corresponding element signal detected.

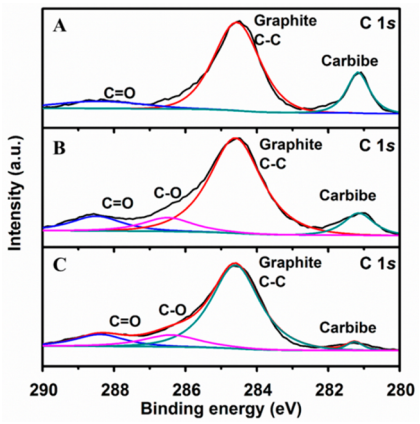

Figure 4. C 2p spectra of (A) Ti_3AlC_2 sample without ant treatment, (B) after treating with 10 wt % HF solution and fully exfoliated, and (C) after treating with Cr (VI).

In contrast to the sheet-like structures of $Ti_3C_2T_x$ nanosheets, Figure 5A shows that the white powders are compose of granular particles with a uniform size of 50 nm. Figure 5B, the XRD of the white powders indicates that they are rutile TiO_2 crystals, according to PDF#21-1276. The corresponding XPS results (Table 1 and Figure 6) further confirm (Figure 6) that

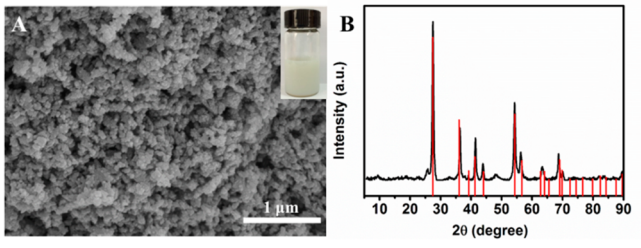

Figure 5. (A) SEM image of the $Ti_3C_2T_x$-10% nanosheets after being stored in a beaker for 3 months. Insert is the corresponding photo. (B) XRD pattern of the white precipitation. The red columns are the standard XRD PDF file of rutile TiO_2.

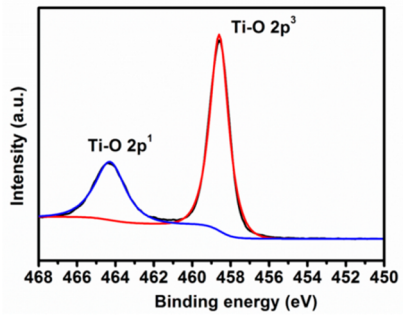

Figure 6. Ti 2p spectrum of the 2-D $Ti_3C_2T_x$ nanosheets after storing for 3 months.

no Ti−C bond exists. Based on the above results, it is obvious that $Ti_3C_2T_x$ nanosheets have been transformed to granular rutile TiO_2 crystals after 3 months under atmospheric conditions. This means that $Ti_3C_2T_x$ nanosheets exhibit reductivity in aqueous solution. The SSA of the $Ti_3C_2T_x$ nanosheets is critically important for their potential applications. SI, Figure S6 shows the nitrogen adsorption−desorption isotherms of the $Ti_3C_2T_x$-10% nanosheets, which are representative type-H3 curves. BET results demonstrate that the 2-D $Ti_3C_2T_x$-10% nanosheets exhibit the highest SSA of 57 $m^2\ g^{-1}$ with a pore volume of 0.11 $cm^3\ g^{-1}$ among the prepared three samples (SI, Figure S6 and Table 2), indicating good

Table 2. Specific Surface Area and Cr(VI) Removal Capacity of 2-D $Ti_3C_2T_x$ Nanosheets Treated with HF Solution of Different Concentrations

sample	$Ti_3C_2T_x$-50%	$Ti_3C_2T_x$-25%	$Ti_3C_2T_x$-10%
BET/$m^2\ g^{-1}$	9	20	57
Cr(VI) removal capacity/ mg g^{-1}	120	170	250

exfoliation in low concentration HF, and are favorable to surface reaction and adsorption. Due to their large surface area, good dispersibility in water, and reductivity, $Ti_3C_2T_x$ nanosheets can be expected to be used for reductive removal of highly toxic, soluble, and strong oxidants, such as Cr(VI), Mn(VII), and so on.

3.2. Removal Capacity for Cr(VI). Cr(VI) is considered as a primary highly toxic pollutant in water and its efficient

DOI: 10.1021/am5074722
ACS Appl. Mater. Interfaces 2015, 7, 1795−1803

removal from water is of great importance. As mentioned above, due to the large SSA, 2-D structure and the reductivity, the 2-D $Ti_3C_2T_x$ nanosheets would be useful for reductive removal of high valence heavy metal ions from wastewater.

The removal performance of toxic Cr(VI) by $Ti_3C_2T_x$ nanosheets was investigated systematically. The Cr(VI) removal capacity of $Ti_3C_2T_x$ was calculated by the following equation:

$$Q = \frac{(C_0 - C_r)V}{m} \quad (1)$$

where Q represents the Cr(VI) removal capacity of $Ti_3C_2T_x$ (mg g^{-1}) anf C_0 and C_r (mg L^{-1}) are the initial and residual concentrations of Cr(VI) ions in aqueous solution, respectively. V (L) is the volume of aqueous solution and m (g) is the weight of $Ti_3C_2T_x$ nanosheets added into the solution. The residual concentration of Cr(VI) was estimated by UV−vis spectra at 540 nm using 5-diphenyl carbazide.[30]

In order to exclude the uncertain influences on solution pH after adding the $Ti_3C_2T_x$ nanosheets into $K_2Cr_2O_7$ solution, equal volume of $Ti_3C_2T_x$ nanosheets suspension was mixed with $K_2Cr_2O_7$ solution with the same pH at room temperature.

3.2.1. Removal Capacities of Different $Ti_3C_2T_x$ Nanosheets for Cr(VI). The prepared $Ti_3C_2T_x$-10%, $Ti_3C_2T_x$-25%, and $Ti_3C_2T_x$-50% nanosheets were employed to determine the optimum concentration of HF solution via mixing equal volumes of the corresponding $Ti_3C_2T_x$ nanosheets suspension (0.2 g L^{-1}) with $K_2Cr_2O_7$ solution (208 ppm of Cr(VI)) at pH 5.0, respectively. The test lasted for 72 h to confirm the saturated removal capacity of Cr(VI). As shown in Table 2, the $Ti_3C_2T_x$-10% nanosheets, due to their largest SSA, demonstrate the best removal performance of 250 mg g^{-1}, while that of $Ti_3C_2T_x$-50% nanosheets is 170 mg g^{-1} and $Ti_3C_2T_x$-25% nanosheets is 120 mg g^{-1}. This performance is comparable to other competitors (Table 3).[31−45]

3.2.2. Effect of the Amount of $Ti_3C_2T_x$ Nanosheets. The dosage effect of $Ti_3C_2T_x$-10% nanosheets suspension on the removal performance of Cr(VI) was further investigated at pH 5.0. Figure 7A shows the time-dependence removal performance of Cr(VI) over the dosage effect of $Ti_3C_2T_x$-10% nanosheets. At the initial stage, the removal rate is very fast because of sufficient reaction active sites on the surfaces of $Ti_3C_2T_x$-10% nanosheets and sufficient concentration of Cr(VI) species. Subsequently, it slows down as the active sites and the concentration of Cr(VI) decrease. Moreover, the removal rate of Cr(VI) increased with the amount of $Ti_3C_2T_x$-10% nanosheets increased from 0.2 to 1.0 g L^{-1}. When an equal volume of 0.4 g L^{-1} $Ti_3C_2T_x$-10% nanosheets were employed, the concentration of Cr(VI) was significantly decreased from 208 ppm to less than 5 ppb in the residual solution within 2 h, which nearly reached the detection limit of the UV−vis method.

3.2.3. Effect of the pH. It is well-known that potassium dichromate is a powerful oxidant at low pH or neutral solution.[46] The reduction half-reaction equation can be written as follows:

$$Cr_2O_7^{2-}(aq) + 14H^+ + 6e^- \rightarrow 2Cr^{3+}(aq) + 7H_2O \quad (E = +1.33V) \quad (2)$$

As expected, Figure 7B shows that the removal rate of Cr(VI) is remarkably pH-dependent. The lower the pH, the quick the removal rate is. The Cr(VI) removal capacity degraded quickly with the increase of pH value. The nanosheets nearly lost the Cr(VI) removal ability at pH 13.0. Cr(VI) is reduced to Cr(III) under the acidic environment by $Ti_3C_2T_x$-10% nanosheets, demonstrating that they serve as electron donors. The product of reduction, Cr(III), can be anchored on the surface of $Ti_3C_2T_x$ nanosheets at the same time. ICP-AES results show that the total Cr in the residual solution is only 2.0 ppm at pH 5.0. The color of the final solution turned from yellow to colorless, which confirmed the combination of the reduction and adsorption processes together. It meant that the highly toxic Cr(VI) was successfully converted to less toxic Cr(III), and the later was readily removed by in situ adsorption, which was further confirmed by XPS and ICP-AES results in the next text.

Table 3. Summary of the Maximum Cr(VI) Removal Capacities of Different Materials[a]

materials	Cr (VI) removal capacity (mg g^{-1})	ref
$Ti_3C_2T_x$ nanosheets	250	this work
ED-rGO	100	31
mesoporous magnetic carbon nanocomposite	3.74	32
aluminum−magnesium mixed hydroxide	105.3−112.0	33
activated carbon	112.36	34
graphene nanocomposites	1.03	35
commercial α-Fe_2O_3	0.68	36
commercial CeO_2	0.37	37
α-Fe_2O_3 nanorods	29.52	38
TiO_2 particles	5	39
anion exchange resin DEX-Cr	248	40
"flower-like" PA6@$Mg(OH)_2$ electrospun nanofibers	294	41
iron oxide submicron wires	0.52	42
PEI/ECs composites	36.8	43
cellulose derived magnetic mesoporous carbon nanocomposites (MC-Fe_3O_4)	293.8	44
cellulose derived magnetic mesoporous carbon nanocomposites (MC-$Fe(NO_3)_3$)	327.5	
polyaniline coating on carbon fiber	18.1	45
sodium hydrogen sulfite	<250[b]	in theory
sodium metabisulfite	<330[c]	in theory
ferrous sulfate	<62.5[d]	in theory

[a]The Cr(VI) removal capacity of sodium hydrogen sulfite, sodium metabisulfite and ferrous sulfate are calculated by the reaction equation, respectively. [b]$2H_2Cr_2O_7 + 6NaHSO_3 + 6HCl = 2Cr_2(SO_4)_3 + 6NaCl + 8H_2O$. [c]$Na_2S_2O_5 + H_2O = 2NaHSO_3$, $2H_2Cr_2O_7 + 6NaHSO_3 + 6HCl = 2Cr_2(SO_4)_3 + 6NaCl + 8H_2O$. [d]$14H^+ + 6Fe^{2+} + +Cr_2O_7^{2-} = 6Fe^{3+} + 2Cr^{3+} + 7H_2O$.

The pH of the mixing solution before and after the removal of Cr(VI) was increased in acidic environment and decreased in alkaline environment, for example, from 2.0 to 2.2, 5.0 to 5.4, 13.0 to 11.6, respectively. The variation of pH was related to the consumption of protons and the hydroxyls during the reaction.

3.3. Chromium Removal Mechanisms. In order to gain further insight into the removal mechanism of Cr(VI), the bonding states of C 1s, Ti 2p, O 1s, and Cr 2p were characterized by XPS. The oxygen states of the sample before and after reacting with Cr(VI) have been analyzed. The O 1s is composed of two peaks, same as the reported result.[27] The peak located at 632 eV is assigned to the hydroxyl groups of 2-

DOI: 10.1021/am5074722
ACS Appl. Mater. Interfaces 2015, 7, 1795−1803

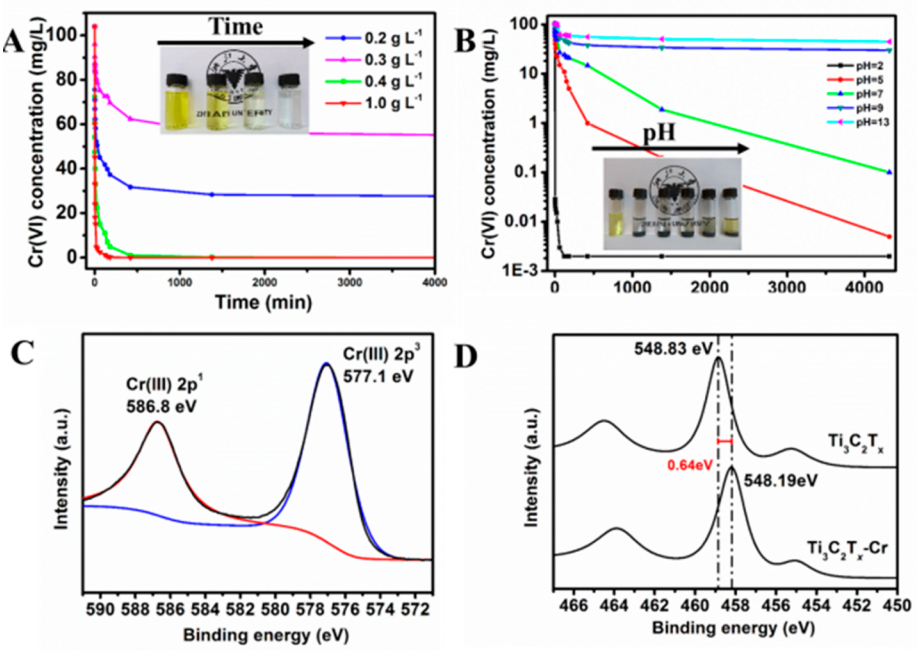

Figure 7. (A) Dosage effect of the $Ti_3C_2T_x$-10% nanosheets on the removal of Cr (VI) in 400 mL of 104 mg L^{-1} solution (pH 5.0). Insert is the corresponding photo with elongation of time, indicating the change in color in the case of 0.4 g L^{-1} $Ti_3C_2T_x$-10% nanosheets. (B) Removal of Cr (VI) in 400 mL of 104 mg L^{-1} solution ($Ti_3C_2T_x$-10% nanosheets concentration: 0.4 g L^{-1}) dependent on pH. Insert is the final solution color at different pH. (C) Cr 2p XPS spectrum of the Cr-loading $Ti_3C_2T_x$-10% nanosheets. (D) Chemical shift of binding energy of Ti 2p before and after immersing in Cr (VI) solution for 72 h.

D $Ti_3C_2T_x$ nanosheets. The other peak at 529.8 is indexed to the lattice oxygen of the TiO_2 network. During the Cr(VI) removal process, the amount of hydroxyl groups on the $Ti_3C_2T_x$ surface decreases gradually, SI, Figures S4 and S7. For $Ti_3C_2T_x$-10% nanosheets after reacting with Cr(VI), the Cr 2p peak can only be Gaussian-fitted with two peaks with binding energies at 577.1 and 586.8 eV, both of which are attributed to Cr(III) (Figure 7C).[22] No Cr(VI) is detected. These results indicate that all the Cr(VI) has been converted to Cr(III), which agrees with the UV−vis results. In addition, a significant shift of 0.64 eV of Ti 2p to lower binding energy, as observed in Figure 7D, confirms the presence of strong interaction between Cr(III) and Ti−O.[47,48] While the decrease of the peak intensity at 281 eV indicates the breaking of the Ti−C bond during the reduction process (Figure 4).

The reduction and adsorption mechanism are illustrated in Scheme 1. First, because the surfaces of 2-D $Ti_3C_2T_x$-10% nanosheets are terminated with abundant oxygen-containing groups, such as OH, and F (Table 1), the presence of Ti−OH and Ti−F.[15] Zeta potential test indicates that the isoelectric points of $Ti_3C_2T_x$-10% nanosheets is about 2.36 (Figure 8).

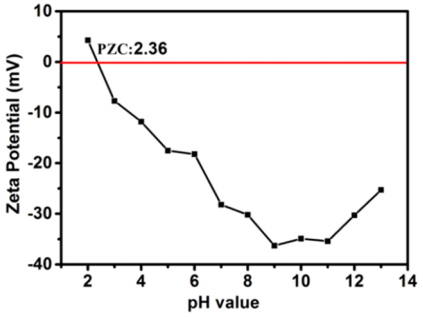

Figure 8. Zeta potential of 0.1 mg mL^{-1} $Ti_3C_2T_x$-10% suspension depends on pH.

Scheme 1. Illustration of the Removal Mechanism of Cr(VI) by the $Ti_3C_2T_x$ Nanosheets

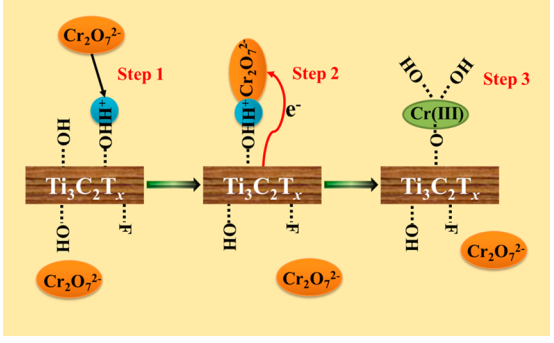

Since the pH of solution (pH 2.0) is below the isoelectric points, the surface of the nanosheets will be positively charged due to the presence of abundant protonated hydroxyl groups,[49] which is evidenced by the XPS result (Figure 4 and SI, Figure S4). The strong electrostatic attraction accelerated the removal of negatively charged $Cr_2O_7^{2-}$. As the pH increased, the removal rate slowed down due to the weakness of electrostatic attraction. Second, after contacting with the surface of $Ti_3C_2T_x$, reduction will be initiated with the assistance of H^+ and the electrons will be transferred from $Ti_3C_2T_x$ to Cr(VI). Theoretically, $Cr(OH)_3$ starts to be precipitated from a 2 mM Cr^{3+} solution at pH 4.8 and completely precipitated at pH 5.6, calculated from K_{sp} ($Cr(OH)_3$: $K_{sp} = 6.3 \times 10^{-31}$).[50] However, we found that $Ti_3C_2T_x$ nanosheets could not remove Cr(III) from $CrCl_3$ solution at pH 5.0 up to 98%. It is strange

DOI: 10.1021/am5074722
ACS Appl. Mater. Interfaces 2015, 7, 1795−1803

that residual Cr in the form of Cr(III) is almost undetectable by ICP-AES in the solution at pH 5.0. Hence, we suggested that the excellent removal performance of the produced Cr(III) at pH 5.0 should be enhanced by the [Ti−O] bond, which have high sorption affinity toward metallic ions.[15] The produced Cr(III) are partly anchored on the surface of the sheets via covalent bonds with [Ti−O] bond simultaneously and formed Ti−O−Cr(III) at last, which is consistent with the result that only 2% of Cr element at pH 5.0 but 98% at pH 2.0 in the residual solution after 72 h. The shift of the Ti 2p peak verified the presence of Ti−O−Cr bond as mentioned above. In alkaline environment, the oxidizability of Cr(VI) was very weak.[51] The color of $Ti_3C_2T_x$ nanosheets suspension turned from black to gray and lost the removal ability. Since the removal of Cr(VI) by $Ti_3C_2T_x$ nanosheets is through a reductive reaction, it is very difficult to recover the removal capacity for Cr(VI) after releasing the adsorbed Cr(III) by 10 mM HCl solution.

3.4. Removal of Other Oxidants. $Ti_3C_2T_x$ nanosheets were further used for the reductive removal of other oxidant agents. The results show that the $K_3[Fe(CN)_6]$ (yellow), $KMnO_4$ (purple) and $NaAuCl_4$ (yellow) solutions can easily be reduced by mixing with 2-D $Ti_3C_2T_x$ nanosheets suspension (Figure 9). After stirring for a certain time, the colors in all

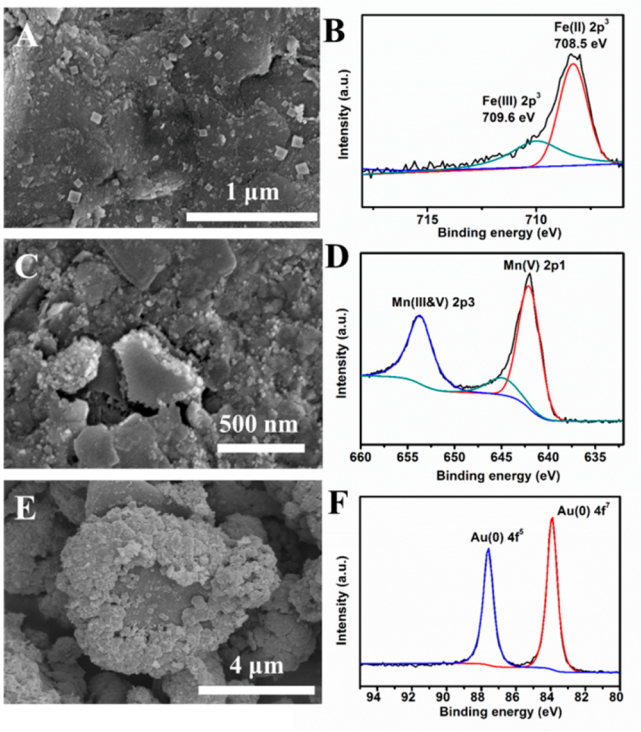

Figure 9. XPS spectra and SEM images of 2-D $Ti_3C_2T_x$ nanosheets after reacting with (A and B) $K_3[Fe(CN)_6]$, (C and D) $KMnO_4$, and (E and F) $NaAuCl_4$ solution.

oxidant solution faded away, indicating a reduction was occurring. For example, the color of the $K_3[Fe(CN)_6]$ solution turned from yellow to green because Fe(III) has been reduced to Fe(II) after mixing with $Ti_3C_2T_x$, which was confirmed by XPS results (Figure 9B). When $KMnO_4$ was employed, the Ti−C peak totally disappeared in the XPS spectrum (Figure 10), and Mn(VII) was reduced to Mn(III) and Mn(V) (Figure 9D). In the case of $HAuCl_4$, the 2-D nanosheets were surrounded

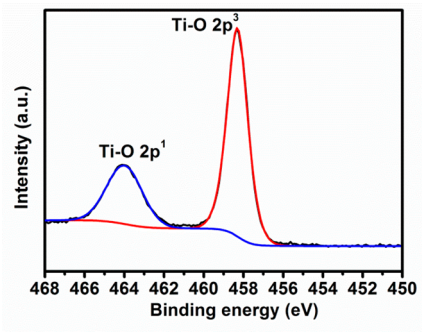

Figure 10. Ti 2p spectra of the 2-D $Ti_3C_2T_x$ nanosheets after mixing with $KMnO_4$.

with gold particles (Figure 9E,F). This provides a method to load noble metals on these 2-D nanosheets and holds the potential to be used in catalysis.

4. CONCLUSIONS

In summary, novel 2-D $Ti_3C_2T_x$ nanosheets prepared by an intercalation and exfoliation process exhibit excellent removal capacity for toxic Cr(VI). The max removal capacity is 250 mg g^{-1} by $Ti_3C_2T_x$-10% nanosheets, which is comparable to other competitors. More importantly, the Cr(VI) can be effectively reduced to less toxic Cr(III) species and the residual Cr(VI) in treated water was far below the drinking water standard recommended by the WHO. At the same time, the resulting Cr(III) can be removed without any alkali treatment at pH 5.0. Moreover, we systematically investigate the effect of pH on the Cr(VI) removal performance and find the optimum conditions at pH 5, which has the best Cr(VI) and Cr(III) removal performance. Based on their high surface area, well dispersibility, and reductivity, these $Ti_3C_2T_x$ nanosheets are promising candidates for removal of toxic high valent metal ion related oxidants from wastewater.

■ ASSOCIATED CONTENT

Supporting Information

SEM images of the samples, including untreated Ti_3AlC_2 powders, Ti_3AlC_2 samples after treating with different concentrations of HF and after full exfoliation, $Ti_3C_2T_x$-10% nanosheets at low magnification. O 1s and F1s XPS spectra of the 2-D $Ti_3C_2T_x$ nanosheets, and O 1s spectrum of the 2-D $Ti_3C_2T_x$ nanosheets after treated with Cr(VI), and N_2 adsorption−desorption isotherms. This material is available free of charge via the Internet at http://pubs.acs.org.

■ AUTHOR INFORMATION

Corresponding Author

*E-mail: pengxinsheng@zju.edu.cn.

Notes

The authors declare no competing financial interest.

■ ACKNOWLEDGMENTS

This work was supported by the National Natural Science Foundations of China (NSFC 21271154), the National Basic Research Program of China 973 Program (2015CB655302), and Natural Science Foundation for Outstanding Young Scientist of Zhejiang Province, China (LR14E020001).

DOI: 10.1021/am5074722
ACS Appl. Mater. Interfaces 2015, 7, 1795−1803

REFERENCES

(1) Butler, S. Z.; Hollen, S. M.; Cao, L. Y.; Cui, Y.; Gupta, J. A.; Gutierrez, H. R.; Heinz, T. F.; Hong, S. S.; Huang, J. X.; Ismach, A. F.; Johnston-Halperin, E.; Kuno, M.; Plashnitsa, V. V.; Robinson, R. D.; Ruoff, R. S.; Salahuddin, S.; Shan, J.; Shi, L.; Spencer, M. G.; Terrones, M.; Windl, W.; Goldberger, J. E. Progress, Challenges, and Opportunities in Two-Dimensional Materials Beyond Graphene. *ACS Nano* **2013**, *7*, 2898−2926.

(2) Xu, M. S.; Liang, T.; Shi, M. M.; Chen, H. Z. Graphene-Like Two-Dimensional Materials. *Chem. Rev.* **2013**, *113*, 3766−3798.

(3) Huang, H. B.; Song, Z. G.; Wei, N.; Shi, L.; Mao, Y. Y.; Ying, Y. L.; Sun, L. W.; Xu, Z. P.; Peng, X. S. Ultrafast Viscous Water Flow through Nanostrand-channelled Graphene Oxide Membranes. *Nat. Commun.* **2013**, *4*, 2979.

(4) Mi, B. X. Graphene Oxide Membranes for Ionic and Molecular Sieving. *Science* **2014**, *343*, 740−742.

(5) Ying, Y. L.; Sun, L. W.; Wang, Q.; Fan, Z. J.; Peng, X. S. In-plane Mesoporous Graphene Oxide Nanosheet Assembled Membranes for Molecular Separation. *RSC Adv.* **2014**, *4*, 21425−21428.

(6) Sun, L. W.; Ying, Y. L.; Huang, H. B.; Song, Z. G.; Mao, Y. Y.; Xu, Z. P.; Peng, X. S. Ultrafast Molecule Separation through Layered WS_2 Nanosheet Membranes. *ACS Nano* **2014**, *8*, 6304−6311.

(7) Naguib, M.; Mashtalir, O.; Carle, J.; Presser, V.; Lu, J.; Hultman, L.; Gogotsi, Y.; Barsoum, M. W. Two-Dimensional Transition Metal Carbides. *ACS Nano* **2012**, *6*, 1322−1331.

(8) Mashtalir, O.; Naguib, M.; Mochalin, V. N.; Dall'Agnese, Y.; Heon, M.; Barsoum, M. W.; Gogotsi, Y. Intercalation and Delamination of Layered Carbides and Carbonitrides. *Nat. Commun.* **2013**, *4*, 1716.

(9) Lukatskaya, M. R.; Mashtalir, O.; Ren, C. E.; Dall'Agnese, Y.; Rozier, P.; Taberna, P. L.; Naguib, M.; Simon, P.; Barsoum, M. W.; Gogotsi, Y. Cation Intercalation and High Volumetric Capacitance of Two-dimensional Titanium Carbide. *Science* **2013**, *341*, 1502−1505.

(10) Naguib, M.; Kurtoglu, M.; Presser, V.; Lu, J.; Niu, J.; Heon, M.; Hultman, L.; Gogotsi, Y.; Barsoum, M. W. Two-dimensional Nanocrystals Produced by Exfoliation of Ti_3AlC_2. *Adv. Mater.* **2011**, *23*, 4248−4253.

(11) Spanier, J. E.; Gupta, S.; Amer, M.; Barsoum, M. W. Vibrational Behavior of the $M_{n+1}AX_n$ Phases from First-order Raman Scattering (M=Ti,V,Cr, A=Si, X=C,N). *Phys. Rev. B* **2005**, *71*, 012103.

(12) Naguib, M.; Come, J.; Dyatkin, B.; Presser, V.; Taberna, P.-L.; Simon, P.; Barsoum, M. W.; Gogotsi, Y. MXene: A Promising Transition Metal Carbide Anode for Lithium-ion Batteries. *Electrochem. Commun.* **2012**, *16*, 61−64.

(13) Xie, X.; Chen, S.; Ding, W.; Nie, Y.; Wei, Z. An Extraordinarily Stable Catalyst: Pt NPs Supported on Two-dimensional $Ti_3C_2X_2$ (X = OH, F) Nanosheets for Oxygen Reduction Reaction. *Chem. Commun.* **2013**, *49*, 10112−10114.

(14) Come, J.; Naguib, M.; Rozier, P.; Barsoum, M. W.; Gogotsi, Y.; Taberna, P. L.; Morcrette, M.; Simon, P. A Non-Aqueous Asymmetric Cell with a Ti_2C-Based Two-Dimensional Negative Electrode. *J. Electrochem. Soc.* **2012**, *159*, A1368−A1373.

(15) Peng, Q.; Guo, J.; Zhang, Q.; Xiang, J.; Liu, B.; Zhou, A.; Liu, R.; Tian, Y. Unique Lead Adsorption Behavior of Activated Hydroxyl Group in Two-dimensional Titanium Carbide. *J. Am. Chem. Soc.* **2014**, *136*, 4113−4116.

(16) Owlad, M.; Aroua, M. K.; Daud, W. A. W.; Baroutian, S. Removal of Hexavalent Chromium-Contaminated Water and Wastewater: A Review. *Water Air Soil Pollut.* **2009**, *200*, 59−77.

(17) Kimbrough, D. E.; Cohen, Y.; Winer, A. M.; Creelman, L.; Mabuni, C. A Critical Assessment of Chromium in the Environment. *Crit. Rev. Environ. Sci. Technol.* **1999**, *29*, 1−46.

(18) World Health Organization *Guidelines for Drinking-water Quality*, 4th ed.; World Health Organization: Geneva, 2011; Vol. *8*, p 186.

(19) Beaumont, J. J.; Sedman, R. M.; Reynolds, S. D.; Sherman, C. D.; Li, L. H.; Howd, R. A.; Sandy, M. S.; Zeise, L.; Alexeeff, G. V. Cancer Mortality in a Chinese Population Exposed to Hexavalent Chromium in Drinking Water. *Epidemiology* **2008**, *19*, 12−23.

(20) Shanker, A. K.; Cervantes, C.; Loza-Tavera, H.; Avudainayagam, S. Chromium Toxicity in Plants. *Environ. Int.* **2005**, *31*, 739−753.

(21) Barrera-Diaz, C. E.; Lugo-Lugo, V.; Bilyeu, B. A Review of Chemical, Electrochemical and Biological Methods for Aqueous Cr(VI) Reduction. *J. Hazard. Mater.* **2012**, *223−224*, 1−12.

(22) Guo, X. A.; Fei, G. T.; Su, H.; Zhang, L. D. High-Performance and Reproducible Polyaniline Nanowire/Tubes for Removal of Cr(VI) in Aqueous Solution. *J. Phys. Chem. C* **2011**, *115*, 1608−1613.

(23) Rengaraj, S.; Joo, C. K.; Kim, Y.; Yi, J. Kinetics of Removal of Chromium from Water and Electronic Process Wastewater by Ion Exchange Resins: 1200H, 1500H and IRN97H. *J. Hazard. Mater.* **2003**, *102*, 257−275.

(24) Hafez, A.; El-Mariharawy, S. Design and Performance of the Two-stage/two-pass RO Membrane System for Chromium Removal from Tannery Wastewater. Part 3. *Desalination* **2004**, *165*, 141−151.

(25) Marder, L.; Bernardes, A. M.; Zoppas Ferreira, J. Cadmium Electroplating Wastewater Treatment Using a Laboratory-scale Electrodialysis System. *Sep. Purif. Technol.* **2004**, *37*, 247−255.

(26) Hu, Z.; Lei, L.; Li, Y.; Ni, Y. Chromium Adsorption on High-performance Activated Carbons from Aqueous Solution. *Sep. Purif. Technol.* **2003**, *31*, 13−18.

(27) Kubacka, A.; Bachiller-Baeza, B.; Colon, G.; Fernandez-Garcia, M. Doping Level Effect on Sunlight-Driven W, N-Co-Doped Tio2-Anatase Photo-Catalysts for Aromatic Hydrocarbon Partial Oxidation. *Appl. Catal., B* **2010**, *93*, 274−281.

(28) Wu, G. S.; Wang, J. P.; Thomas, D. F.; Chen, A. C. Synthesis of F-Doped Flower-Like Tio2 Nanostructures with High Photoelectrochemical Activity. *Langmuir* **2008**, *24*, 3503−3509.

(29) Myhra, S.; Crossley, J.; Barsoum, M. Crystal-chemistry of the Ti_3AlC_2 and Ti_4AlN_3 Layered Carbide/nitride Phases—Characterization by XPS. *J. Phys. Chem. Solids* **2001**, *62*, 811−817.

(30) Wang, L.; Bian, G. R.; Dong, L.; Xia, T. T.; Hong, S.; Chen, H. Q. Selective Fluorescence Determination of Chromium (VI) in Water Samples with Terbium Composite Nanoparticles. *Spectrochim. Acta Part A* **2006**, *65*, 123−126.

(31) Ma, H. L.; Zhang, Y. W.; Hu, Q. H.; Yan, D.; Yu, Z. Z.; Zhai, M. L. Chemical Reduction and Removal of Cr(VI) from Acidic Aqueous Solution by Ethylenediamine-reduced Graphene Oxide. *J. Mater. Chem.* **2012**, *22*, 5914−5916.

(32) Zhu, J. H.; Gu, H. B.; Guo, J.; Chen, M. J.; Wei, H. G.; Luo, Z. P.; Colorado, H. A.; Yerra, N.; Ding, D.; Ho, T. C.; Haldolaarachchige, N.; Hopper, J.; Young, D. P.; Guo, Z. H.; Wei, S. Y. Mesoporous Magnetic Carbon Nanocomposite Fabrics for Highly Efficient Cr(VI) Removal. *J. Mater. Chem. A* **2014**, *2*, 2256−2265.

(33) Li, Y. J.; Gao, B. Y.; Wu, T.; Sun, D. J.; Li, X.; Wang, B.; Lu, F. J. Hexavalent Chromium Removal from Aqueous Solution by Adsorption on Aluminum Magnesium Mixed Hydroxide. *Water Res.* **2009**, *43*, 3067−3075.

(34) EI-Sikaily, A.; El Nemr, A.; Khaled, A.; Abdelwehab, O. Removal of Toxic Chromium from Wastewater Using Green Alga Ulva Lactuca and Its Activated Carbon. *J. Hazard. Mater.* **2007**, *148*, 216−228.

(35) Zhu, J. H.; Wei, S. Y.; Gu, H. B.; Rapole, S. B.; Wang, Q.; Luo, Z. P.; Haldolaarachchige, N.; Young, D. P.; Guo, Z. H. One-Pot Synthesis of Magnetic Graphene Nanocomposites Decorated with Core@Double-shell Nanoparticles for Fast Chromium Removal. *Environ. Sci. Technol.* **2012**, *46*, 977−985.

(36) Zhong, L. S.; Hu, J. S.; Liang, H. P.; Cao, A. M.; Song, W. G.; Wan, L. J. Self-assembled 3D Flowerlike Iron Oxide Nanostructures and Their Application in Water Treatment. *Adv. Mater.* **2006**, *18*, 2426−2431.

(37) Zhong, L. S.; Hu, J. S.; Cao, A. M.; Liu, Q.; Song, W. G.; Wan, L. J. 3D Fowerlike Ceria Micro/nanocomposite Structure and Its Application for Water Treatment and CO Removal. *Chem. Mater.* **2007**, *19*, 1648−1655.

(38) Tel, H.; Altas, Y.; Taner, M. S. Adsorption Characteristics and Separation of Cr(III) and Cr(VI) on Hydrous Titanium(IV) Oxide. *J. Hazard. Mater.* **2004**, *112*, 225−231.

DOI: 10.1021/am5074722
ACS Appl. Mater. Interfaces 2015, 7, 1795−1803

(39) Liu, E.-t.; Zhao, H.; Li, H.; Li, G.; Liu, Y.; Chen, R. Hydrothermal Synthesis of Porous α-Fe2O3 Nanostructures for Highly Efficient Cr(VI) Removal. *New J. Chem.* **2014**, *38*, 2911.
(40) Liu, X.; Li, Y.; Wang, C.; Ji, M. Cr(VI) Removal by a New Type of Anion Exchange Resin DEX-Cr: Adsorption Affecting Factors, Isotherms, Kinetics, and Desorption Regeneration. *Environ. Progress Sust. Energy* **2014**, DOI: 10.1002/ep.11998.
(41) Jia, B.-B.; Wang, J.-N.; Wu, J.; Li, C.-J. Flower-Like" PA6@ $Mg(OH)_2$ Electrospun Nanofibers with Cr (VI)-removal Capacity. *Chem. Eng. J.* **2014**, *254*, 98−105.
(42) Liu, Z.; Chen, L.; Zhang, L.; Poyraz, S.; Zhang, X.; Zhu, J. Ultrafast Cr (VI) Removal from Polluted Water by Microwave Synthesized Iron Oxide Submicron Wires. *Chem. Commun.* **2014**, *50*, 8036−8039.
(43) Qiu, B.; Guo, J.; Zhang, X.; Sun, D.; Gu, H.; Wang, Q.; Wang, H.; Wang, X.; Zhang, X.; Weeks, B. L.; Guo, Z.; Wei, S. Polyethylenimine Facilitated Ethyl Cellulose for Hexavalent Chromium Removal with a Wide pH Range. *ACS Appl. Mater. Interfaces* **2014**, *6*, 19816−19824.
(44) Qiu, B.; Gu, H. B.; Yan, X. R.; Guo, J.; Wang, Y. R.; Sun, D. Z.; Wang, Q.; Khan, M.; Zhang, X.; Weeks, B. L.; Young, D. P.; Guo, Z. H.; Wei, S. Y. Cellulose Derived Magnetic Mesoporous Carbon Nanocomposites with Enhanced Hexavalent Chromium Removal. *J. Mater. Chem. A* **2014**, *2*, 17454−17462.
(45) Qiu, B.; Xu, C. X.; Sun, D. Z.; Wei, H. G.; Zhang, X.; Guo, J.; Wang, Q.; Rutman, D.; Guo, Z. H.; Wei, S. Y. Polyaniline Coating on Carbon Fiber Fabrics for Improved Hexavalent Chromium Removal. *RSC Adv.* **2014**, *4*, 29855−29865.
(46) Weckhuysen, B. M.; Wachs, I. E.; Schoonheydt, R. A. Surface Chemistry and Spectroscopy of Chromium in Inorganic Oxides. *Chem. Rev.* **1996**, *96*, 3327−3349.
(47) Zhang, X.; Lei, L.; Zhang, J.; Chen, Q.; Bao, J.; Fang, B. Preparation of PW12O403−/Cr−TiO_2 Nanotubes Photocatalysts with the High Visible Light Activity. *Sep. Purif. Technol.* **2009**, *67*, 50−57.
(48) Hussain, S. T.; Siddiqa, A. Iron and Chromium Doped Titanium Dioxide Nanotubes for the Degradation of Environmental and Industrial Pollutants. *Inter. J. Environ. Sci. Technol.* **2011**, *8*, 351−362.
(49) Hsu, H.-T.; Chen, S.-S.; Chen, Y.-S. Removal of Chromium(VI) and Naphthalenesulfonate from Textile Wastewater by Photocatalysis Combining Ionic Exchange Membrane Processes. *Sep. Purif. Technol.* **2011**, *80*, 663−669.
(50) Yang, J.; Peng, J.; Liu, K.; Guo, R.; Xu, D.; Jia, J. Synthesis of Ferrites Obtained from Heavy Metal Solutions Using Wet Method. *J. Hazard. Mater.* **2007**, *143*, 379−385.
(51) Cui, J.; Wang, Z. M.; Liu, F. L.; Dai, P. B.; Chen, R.; Zhou, H. Y. Preparation of Persimmon Tannins Immobilized on Collagen Adsorbent and Research on its Adsorption to Cr(VI). *Mater. Sci. Form* **2013**, *743*−*744*, 523−530.

DOI: 10.1021/am5074722
ACS Appl. Mater. Interfaces 2015, 7, 1795−1803